ACS APPLIED MATERIALS & INTERFACES

Research Article

www.acsami.org

Role of Hot Singlet Excited States in Charge Generation at the Black Dye/TiO_2 Interface

Ajay Ram Srimath Kandada,[†] Simona Fantacci,[‡] Simone Guarnera,[†,§] Dario Polli,[†] Guglielmo Lanzani,[†,§] Filippo De Angelis,*[,‡] and Annamaria Petrozza*[,§]

[†]Dipartimento di Fisica, Politecnico di Milano, Piazza Leonardo da Vinci 32, 20133 Milano, Italy

[‡]Computational Laboratory for Hybrid/Organic Photovoltaics (CLHYO), Istituto CNR di Scienze e Tecnologie Molecolari, Via Elce di Sotto 8, I-06123, Perugia, Italy

[§]Center for Nano Science and Technology @ PoliMi, Istituto Italiano di Tecnologia, via Pascoli 70/3 20133 Milano, Italy

Supporting Information

ABSTRACT: Photoinduced electron transfer at low-band-gap ruthenium-based dye/TiO_2 has been investigated by means of ultrafast transient absorption and DFT/TDDFT calculations. We demonstrate that although the charge generation mechanism is triplet mediated upon band gap excitation, as already proven in high band gap dyes such as the well-known N3 and N719, when excess energy is provided which allows to reach high energy singlet states still in the visible spectral range, ultrafast electron transfer takes place. No intersystem crossing process is observed and charge generation happens only from the singlet excited state.

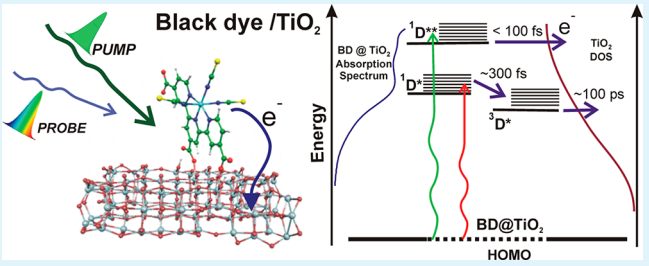

KEYWORDS: *black dye, DSSC, charge generation, hot injection, DFT, transient absorption*

INTRODUCTION

Since the first report of efficient dye-sensitized solar cells (DSC),[1] the optoelectronic processes at the interface between the N3 dye and nanocrystalline TiO_2 films or I^-/I^-_3 redox couple have been largely investigated, as it has been considered the prototypal system for this class of solar cells. These studies have led to gaining more and more fundamental knowledge on the working mechanism of DSC. One of the major issues for further improvement in the DSCs is the design of panchromatic sensitizers, which absorb the lower energy region of the visible radiation spectrum up to near-IR (NIR). In this respect, the $[Ru(H_3tcterpy)(NCS)_3]^-$ (tcterpy=4,4′,4″-tricarboxy-2,2′:6′,2″-terpyridine), also known as N749 or black dye (BD), has attracted considerable experimental interest.[2,3] As a matter of fact, the BD is nowadays employed in DSSC, which provides the highest certified efficiency of 11.4%.[4,5] Though there is large interest for this dye, very little is known on its photophysical behavior. Pushing the absorption edge of the molecule toward the near-IR can induce important changes in the electronic landscape of the sensitizer and in all the optoelectronic processes related to the interface.[6,7] Most of the time, an efficient design of the hybrid interface in the presence of low-band gap dyes is a critical issue because of the need of always compromising between good solar spectrum match, good open circuit voltage, and good energy level alignment at the interfaces, which will influence the electron/hole transfer rate.

Photoinduced electron injection in nanocrystalline TiO_2 films has been deeply studied in mesoporous metal oxide samples sensitized by a variety of ruthenium complexes. It has been shown that the injection rate and hence the cell efficiency vary with the photon energy.[21] For the well-known N3 and N719 dyes, it is generally recognized that the process happens through a two-step mechanism.[8−11] The first step sees an ultrafast (<150 fs) electron injection from the initially populated, vibronically nonthermalized, singlet excited state, ^{1}MLCT. At this stage, electron injection will compete with intramolecular vibrational redistribution[12] and efficient inter system crossing (<100 fs), thus the singlet excitation relaxes into the thermalized[3] MLCT, which is responsible for the slower electron injection step on the order of tens of picoseconds.[13,14,8] It must be noticed that injection shows a distribution of times that has been explained in terms of electron injection through energetically unfavorable sites[15] or from dye aggregates on the metal oxide surface.[16] Very few studies have been reported on the electron injection mechanism in black dye.[17−20]

Katoh et al.[18,19] carried out transient absorption measurements on the BD/TiO_2 system under various environmental conditions concluding that the electron injection may occur from two distinct energy levels. One allows for ultrafast

Received: February 8, 2013
Accepted: April 23, 2013
Published: April 23, 2013

electron injection, which could not be resolved, and one mediates a slower process that was found to be extremely sensitive to the environmental condition. The latter has been explained invoking the close location of this energy level, probably a relaxed triplet state, to the TiO_2 conduction band edge.

Here, for the first time, we elucidate the electron injection process at the BD/TiO_2 interface using ultrafast transient absorption (TA) spectroscopy together with a computational investigation at the DFT/TDDFT level.We clarify the actual nature of the excited states and the energetics relevant to the electron injection at the low band gap dye/TiO_2 interface.

EXPERIMENTAL METHODS

Sample Preparation and Characterization. Nanoporous TiO_2 substrates were deposited on a glass by doctor-blading technique using TiO_2 Dyesol DSL 18NR-T paste and sintered at 500 °C for 30 min. After this process, the substrates were immersed in a 15 mM $TiCl_4$ solution at 70 °C for 30 min and then placed on a hot plate at 550 °C for 45 min. The obtained TiO_2 films were 7 μm thick. Finally, they were immersed in a solution of N749 black dye (0.4 mM, Solaronix) in ethanol containing chenodeoxycholic acid (20 mM, Sigma Aldrich) in order to avoid dye aggregation for 24 h. The sensitized substrates were then rinsed and dried.

Transient Absorption Spectroscopy. For the measurements with 150 fs resolution, visible-light pulses at 540 nm and 610 nm were generated by a home-built noncollinear optical parametric amplifier, starting from a Clark MXR laser system (1 W output power, 1 kHz repetition rate, 150 fs of pulse duration, wavelength at 780 nm).The probe was a white light continuum pulse generated in a a thin (2 mm) sapphire plate. A pump probe setup employing a computer-controlled optical multichannel analyzer enabling single-shot detection at the full 1 kHz repetition rate was used for measuring the normalized transmission change, $\Delta T/T$. Pump pulses were focused in a 200 μm diameter spot with the excitation energy at 50 nJ per pulse. All measurements were performed at room temperature and at a vacuum of about 1×10^{-3} bar . To obtain higher temporal resolutions, we employed a chirping mirror pair to compress the pulses of a couple of NOPAs to about 15 fs and used as pump and the probe.[22] A similar detection system as described above was used to obtain the differential transmission spectra with a temporal resolution of about 20 fs.

Models and Computational Details. The investigation of selected BD adsorption modes was previously reported by us.[23] Here we just focus on the more stable adsorption mode. The geometry was optimized by the PBE exchange-correlation functional,[24] as implanted in the ADF program package.[25] Electronic structure and TDDFT calculations were performed using the B3LYP[26] functional along with 3-21G* and DGDZVP basis sets, as implemented in the Gaussian03 (G03) program package.[27]To simulate the optical absorption spectra up to a significant energy, TDDFT calculations of the 100 lowest singlet−singlet excitations were performed in water solution. To model the TiO_2 surface, we consider a $(TiO_2)_{82}$ cluster, obtained by appropriately "cutting" an anatase slab exposing the majority (101) surface.[28] Following the work by Persson et al.,[29] we consider a neutral stoichiometric TiO_2 cluster with no saturating atoms or groups at the cluster border. These models have been shown to accurately reproduce the electronic and structural properties of TiO_2 anatase.[29] The employed $(TiO_2)_{82}$ model is an almost square TiO_2 (101) two-layer anatase slab of ca. 2 nm side, with three rows of five- and sixcoordinatedsurface Ti sites, which is large enough to avoid possible spurious dye/titania interactions at the cluster border due to the finite cluster size. The calculated dipole moment for our $(TiO_2)_{82}$ cluster is correctly found to be almost vanishing in all directions (0.5, 0.7, and 0.8 D for *x*, *y*, and *z*, the latter corresponding to the surface normal). The $(TiO_2)_{82}$ cluster has been already successfully employed to study the adsorption mode, the electronic structure and the absorption spectrum of N719 on titania,[30,31] we thus can be confident of the accuracy of the TiO_2 model.

RESULTS AND DISCUSSION

Figure 1a shows a comparison of the experimental and TDDFT-calculated (B3LYP/DGDZVP) optical absorption spectra for BD_1H (a typical protonation state of BD, see the Supporting Information) along with a survey of the molecular orbitals constituting the visible transitions. As it can be noticed, the agreement between theory and experiment is excellent, with the calculated spectrum reproducing all the spectral features of the experimental one, apart from a slight blue shift of the entire calculated spectra. We calculate the lowest transition at 717 nm, corresponding to a HOMO→LUMO excitation. At 605 nm we calculate a transition of HOMO-1→LUMO character, corresponding to the 610 nm experimental band, while at 507 nm we calculate a transition of HOMO→LUMO+1 character, which we associate to the 540 nm feature of the experimental spectrum. Thus the 610 and 540 nm bands represent two excited singlet states which differ both in the starting and arriving orbitals. Because the HOMO/HOMO-1 are almost degenerate, their different energy is due to the LUMO/LUMO+1 splitting, which amounts to 0.4−0.5 eV for the protonation states examined here (see the Supporting Information).

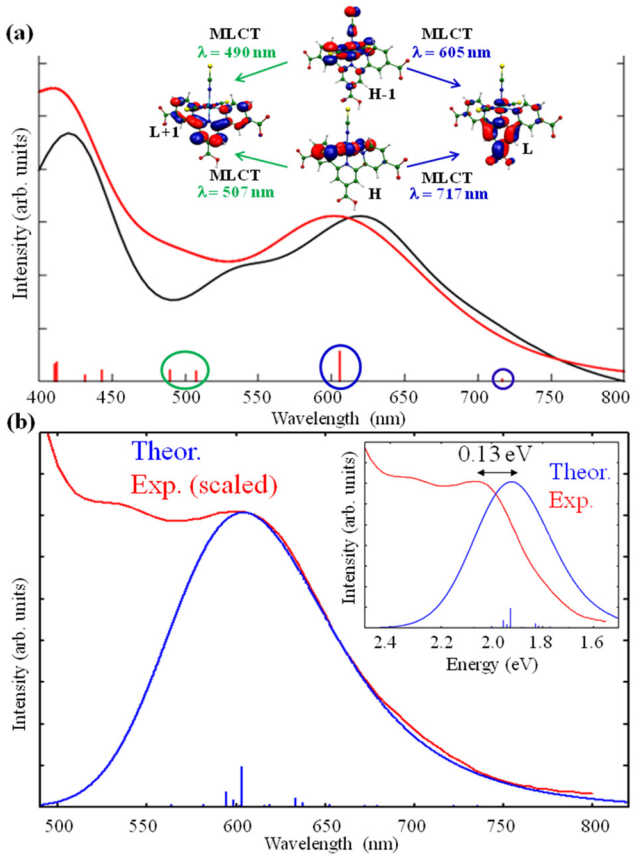

Figure 1. (a) Comparison between calculated (red lines) UV−vis absorption spectrum of BD_1H in water solution with the experimental (black line) spectrum in ethanol. The experimental absorption spectrum has been rescaled to match the intensity of the lowest energy feature of the calculated spectrum. (b) Comparison between the calculated (blue lines) and experimental UV−vis absorption spectra for BD@TiO_2. The calculated spectrum has been blue-shifted by 0.13 eV, corresponding to the difference between the calculated absorption maximum and the experimental one, inset of b.

dx.doi.org/10.1021/am400530v | ACS Appl. Mater. Interfaces 2013, 5, 4334−4339

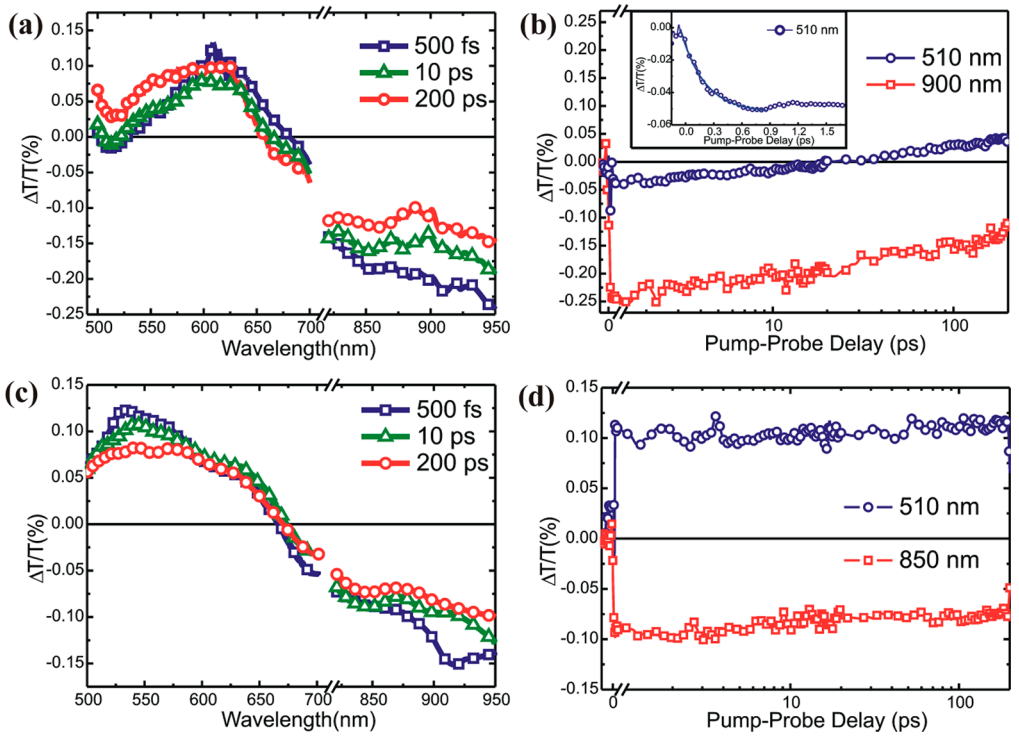

Figure 2. (a) Transient absorption spectra of BD@TiO_2 with the pump wavelength (λ_{pump}) at 610 nm(fluence of 5×10^{14} photons/cm^2/pulse). (b) TA kinetics with λ_{pump} = 610 nm and probe wavelength (λ_{probe}) at 510 and 900 nm. (inset) TA kinetics at λ_{probe} = 510 nm taken with a temporal resolution of 20 fs. (c) TA spectrum with λ_{pump} = 540 nm (fluence of 4.3×10^{14} photons/cm^2/pulse) and (d) associated TA kinetics at λ_{probe} = 510 and 850 nm.

In Figure 1b, we report a comparison of the calculated and experimental UV−vis spectra of BD_2H adsorbed on TiO_2 (BD@TiO_2, see the Supporting Information for the calculated adsorption modes). Because of the large size and complexity of the investigated system, we could calculate "only" the lowest 100 excitation energies in the full TDDFT framework, which limits our discussion to the absorption band experimentally located at 610 nm. Our full TDDFT calculations provide an absorption maximum at 1.90 eV, i.e., only 0.13 eV red-shifted compared to the experimental maximum of 2.03 eV (see inset of Figure 1b). By shifting the calculated absorption spectrum by 0.13 eV, we have essentially a coinciding spectral shape for the calculated and experimental spectra. The lowest transition is calculated at 1.41 eV, with vanishing oscillator strength. This transition corresponds to the direct excitation of one electron from the dye HOMO to the TiO_2 LUMO, corresponding to a fully delocalized state over the semiconductor (see Figure S2 in the Supporting Information). All the higher-lying transitions originate from the dye-based HOMO to higher lying unoccupied orbitals. The lowest transition with a sizable fraction of dye character is found at 1.70 eV, with oscillator strength of 0.003, with the LUMO+4 as arriving state. The main absorption band is constituted by transitions having the LUMO+24 (see Figure S2 in the Supporting Information) to LUMO+53, lying within 0.27 eV, as arriving states. All these states show a strong admixture of dye/semiconductor states, which are originated from the broadening of the isolated dye LUMO after interaction with the semiconductor. Aware of the different nature of the excited states, we proceeded in the investigation of charge generation by selectively exciting different excited states, thus shedding light on the role of excess energy.

Figure 2a shows the TA spectra of BD/TiO2 excited at 610 nm. The TA spectrum, taken with a resolution of 300 fs, shows at a very early time after photoexcitation (500 fs) three main features. For wavelengths (λ) shorter than 550 nm, a negative fractional transmission signal ($\Delta T/T$) that corresponds to a photoinduced absorption (PA) band can be observed. At 550 nm < λ < 690 nm, there is a positive band and for wavelengths longer than 690 nm, another PA band appears. We assign the positive band to the ground-state photobleaching (PB) of the dye. Katoh et al.[17,18] measured the nanosecond TA spectrum of the black dye in acetonitrile and they found a sharp triplet transition, $T_1 \rightarrow T_n$, peaking around 540 nm, and a broad triplet absorption band, less intense, that covers the entire spectral region between 700 nm and 1500 nm. They also measured the ns TA spectrum of the BD/TiO2 sample, for which they found the absorption band of the oxidized dye as a broad feature peaking at 790 nm. On the basis of this evidence, we assign the PA band at λ < 540 nm to a triplet absorption band that overlaps with the PB band. Over time we observe a recovery of the PB band also at short wavelengths, a blue shift of the crossing point of about 30 nm and a decay of the broad band in the near-IR. Figure 2b shows the kinetics taken at 510 nm and 900 nm. At 510 nm, we first observe a decay of the PA that induces a recovery of the PB band after a few tens of picoseconds. At 900 nm, the PA signal decays following the same dynamic of the PA signal at 510 nm. Therefore, we assign the broad PA band in the near IR to triplet absorption as well. Importantly, the triplet decay is associated with a blue shift of the crossing point of the PB band, indicating the feeding of a new excited state population.[8] We thus conclude that when exciting the low energy state at 610 nm, electron injection from the dye to the metal oxide is also mediated by the triplet excited

state in agreement with the well-known picture. However, it is worth noticing that when zooming in the photophysical dynamics by using sub-20 fs resolution pump−probe, we find out that the growing of the triplet population is completed in 0.9 ps with a time constant of about 300 fs (inset in Figure 2b). This reveals an intersystem crossing process much less efficient that the one observed for higher-band-gap ruthenium-based dyes, such as the prototypical $Ru[(bpy)_3]_{2+}$[32] and the related N3/N719 dyes.[8,14]

Figure 2c shows the TA spectra of BD/TiO_2 upon excitation at 540 nm. Strikingly, it reveals that the TA spectrum at very early time after photoexcitation (500 fs) shows only two main features: a PB band for λ < 660 nm and a PA band which extend in the near-IR. The two bands do not evolve in the first tens of ps (see dynamics in Figure 2d) and the crossing point of the fractional change in transmission signal between the PB and PA is already at 660 nm. This is suggesting that by exciting the sensitizer above band gap, at 300 fs no triplet population can be identified, while separated charges can be already probed. Even with sub 20-fs resolution pump probe, no triplet absorption can be observed. We conclude that the generation of charges occurs within 30 fs upon photoexcitation directly from a hot singlet excited state.

A joint representation of the ground and excited energy levels for BD@TiO_2 is reported in Figure 3, where we set the

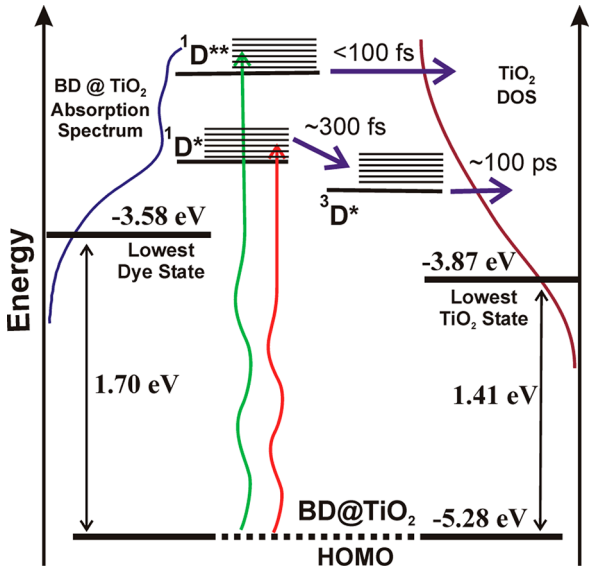

Figure 3. Alignment of the ground and excited states of BD@TiO_2. The experimentally observed injection rates are also indicated when excited at 540 nm (green arrow) and 610 nm (red arrow). The energy levels are not set to scale.

energy of the HOMO (−5.28 eV) as the starting energy for all the transitions. This is fully justified by the fact that all the transitions have the HOMO as starting orbital and that we have shown the HOMO energy to reliably represent the dye oxidation potential. The calculated HOMO energy for BD@TiO_2 is almost coincident with the value of the HOMO calculated for BD_2H at the same B3LYP/3-21G* level (−5.24 eV). We can thus proceed by aligning the (unscaled) UV−vis absorption spectrum for the joint system above the HOMO. We then set the position of the bottom of the TiO_2 conduction band at the lowest dye→semiconductor transition energy (i.e., 1.41 eV above the HOMO) and align the lowest unoccupied Kohn−Sham eigenvalue for BD@TiO_2 to this energy to align the density of states (DOS) of the TiO_2 semiconductor to the joint system's excited states.

As it can be noticed in Figure 3, our calculations provide a conduction band edge energy for TiO_2 of −3.87 eV. Although this value must be treated with some care, we notice that for TiO_2 electrodes in water at pH 7 considering a Nernstian behavior, a flatband energy of −0.58 V vs NHE (−0.82 vs SCE) can be estimated.[33,34] Converting the energy of the NHE reference electrode in water to the vacuum scale, we can position the TiO_2 manifold of unoccupied levels at −3.86 eV vs vacuum, which is almost coincident with our estimate. As it can be noticed in Figure 3, a minimum driving force of ca. 0.3 eV is found for electron injection from the lowest optically active singlet state to the bottom of the TiO_2 manifold of unoccupied states. The absorption maximum experimentally found at 610 nm falls in a region of sizable semiconductor DOS, which is obviously increased for the transitions occurring at higher energy. Assuming that the LUMO+1 of the isolated dye is responsible for the higher energy absorption feature (540 nm) of the TiO_2-adsorbed dye, we do not expect a significantly increased spatial coupling compared to the isolated dye LUMO, which originates the transitions of the TiO_2-adsorbed dye constituting the 610 nm band, because of the similar spatial extension of the two dye orbitals. However, the larger semiconductor DOS sampled by the excited states related to the 540 nm absorption band may justify the hot injection found when exciting at higher energy.

On the other hand, for the isolated dye in solution, the lowest triplet state is found 0.15 eV below the lowest singlet state. In the case of BD@TiO_2, we cannot assign the lowest triplet state based on the dye, due to several overlapping transitions to the dye and to the semiconductor with zero oscillator strength. Assuming the same singlet−triplet splitting for the dye in solution holds for the TiO_2-adsorbed dye, a minimum driving force for electron injection from the triplet state of ca. 0.15 eV is calculated. The reduced driving force should make electron injection from the lowest triplet state much slower than from the corresponding singlet.

It is also interesting to discuss the ISC probability of populating the lowest dye-based triplet state in BD and in the prototype N3 dye as it is exactly the competition between charge injection, internal conversion, and ISC that determines the fate of photoexcitation. In a purely static picture, i.e., neglecting the effects of nuclear dynamics, the ISC probability is directly related to the spin−orbit coupling (SOC) between the singlet and triplet excited-state manifolds. The SOC is introduced in the system by the presence of the heavy transition metal ruthenium center. Because all the excited states originate from the dye-based HOMO to dye or semiconductor unoccupied states with little or none ruthenium character, the SOC can qualitatively be accounted for by the percentage of metal character in the dye HOMO. Recalling that the dye HOMOs both in BD and N3 are made by combinations of ruthenium and NCS states, and by considering that in BD there are three NCS groups, whereas only two NCS groups are present in the N3 dye, we can speculate that a lower ruthenium character is present in the BD HOMO compared to N3. This is precisely verified by our DFT calculations, which provide a percentage of ruthenium states of ∼30 and ∼50% in BD and N3, respectively, with a slight variability introduced by the protonation of the carboxylic groups. It suggests that a lower SOC might characterize the former and is well in agreement

with the slower ISC probability found in the BD compared to N3. This results providential in a system where the singlet excited state has a higher probability of undergo electron transfer to the TiO_2, thanks to a larger semiconductor density of states to sample.

CONCLUSIONS

To summarize, we investigated the charge generation mechanisms in one of the most largely exploited low band gap dyes in DSSC. Expanding the absorption spectrum of the light-harvesting component of the device is of utmost importance in order to achieve a good solar spectrum matching. However, this must be done bearing in mind that the DSSC is a multicomponents system, whose functionality goes beyond the functionally of each single component and strongly depends on the synergy of all of them. In this regard, interface processes are extremely sensitive. First we have elucidated the nature of the excited states involved in charge generation at the dye/TiO_2 interface. Then, we find that excess photon energy with respect to the optical gap is not totally wasted, but is rather exploited to achieve higher electron injection rates. In fact, the lowest singlet transition with no negligible oscillator strength is found to be very close to the metal oxide conduction band, which implies a very little DOS sampled by the excited state. This leads to a rather inefficient electron transfer from the dye singlet state to the TiO_2 and to a competition of this process with ISC between the dyes excited states. It must be noticed that while in other high band gap ruthenium based sensitizers, such as the N3, the electron transfer at the hybrid interface from triplet states has been found quite efficient,[6,15] in the low-band-gap dye, the lowest triplet state results to be too closer to the conduction band of the oxide. This makes the mechanism quite precarious both because of the very slow rate due to very little driving force and because of the sensitiveness to the environment of the actual conduction band position (e.g., solvent polarity, ionic additives), which can even hamper the process.[19] On the other hand, higher energy singlet states, which importantly still lie in the visible spectral range, show an extremely fast electron transfer when excited, in such a way that it overcomes any competing process like internal conversion and ISC, leading to direct charge generation without any triplet state mediation.

The elucidated mechanism highlights a scenario which can be generalized when considering low-band gap dyes (fully organic and not). Upon photoexcitation, these dyes often present efficient intramolecular conversion to low energy molecular excitations (e.g., triplet states or intrachain charge transfer states) with a total energy very close or even lower than the TiO_2 conduction band. This makes them very critical states for charge generation at the TiO_2/dye interface. In solid-state DSSC (which mainly use fully organic push−pull dyes) the problem is sometimes eluded by reductive quenching, i.e., the hole transfer from the dye to the molecular hole conductor is very efficient (ps time scale), allowing for charge generation before the molecular excitation relaxes through dissipative channels. This explains why some organic dyes have been found to work better in solid state than in electrolyte-based solar cells, where the hole transfer happens in the ns−us time regime.[35] The black dye (which can be efficiently used only in electrolyte-based DSSCs because of its low absorption coefficient) seems to partially overcome the relaxation of the primary photoexcitation to low energy states by hot electron injection. Although on the one side, the presented studies should drive the attention of the synthetic chemistry community to shed light on the correlation between the photophysical mechanisms observed and the chemical property of the molecules, they also invoke a material-based paradigm shift that can be required to dramatically enhance the performance of devices when low-band-gap dyes are used. The TiO_2 nanoparticles show a density of states (DOS), peculiar to the material itself, that presents intrinsic "trap" states for the injected electrons.[36] A strategic doping of the metal-oxide could lead to a modulation of the DOS in order to address this problem. Another winning solution could be the development of metal oxides such as SnO_2, which presents a deeper conduction band than TiO_2 and in principle should facilitate more efficient electron transfer from all states in the photoexcited dye molecules, if this initial step is problematic.

ASSOCIATED CONTENT

Supporting Information

Electronic structure of the three protonation states of the isolated black dye in solution; adsorption geometry of TiO_2-adsorbed BD. This material is available free of charge via the Internet at http://pubs.acs.org/.

AUTHOR INFORMATION

Corresponding Author

*E-mail: annamaria.petrozza@iit.it; filippo@thch.unipg.it.

Notes

The authors declare no competing financial interest.

ACKNOWLEDGMENTS

AP research is funded by the European Union Seventh Framework Programme [FP7/2007-2013] under grant agreement 316494. A.R.S.K. and G.L. acknowledge the financial support of the Marie-Curie grant under the FP7 Project PITNGA-2009-237900 (ICARUS). F.D.A. and S.F. thank FP7-NMP-2009 project "SANS" and IIT-SEED 2009 Project "HELYOS" for financial support.

REFERENCES

(1) O'Regan, B.; Grätzel, M. *Nature* **1991**, *353*, 737−740.
(2) Péchy, P.; Renouard, T.; Zakeeruddin, S. M.; Humphry-Baker, R.; Comte, P.; Liska, P.; Cevey, L.; Costa, E.; Shklover, V.; Spiccia, L.; Deacon, G. B.; Bignozzi, C. A.; Grätzel, M. *J. Am. Chem. Soc.* **2001**, *123*, 1613−1624.
(3) Nazeeruddin, K.; Pechy, P.; Grätzel, M. *Chem. Commun.* **1997**, *1*, 1705−1706.
(4) Han, L.; Islam, A.; Chen, H.; Malapaka, C.; Chiranjeevi, B.; Zhang, S.; Yang, X.; Yanagida, M. *Energy Environ. Sci.* **2012**, *5*, 6057−6060.
(5) Chiba, Y.; Islam, A.; Watanabe, Y.; Komiya, R.; Koide, N.; Han, L. *Jpn. J. Appl. Phys.* **2006**, *45*, L638−L640.
(6) Listorti, A.; O'Regan, B.; Durrant, J. R. *Chem. Mater.* **2011**, *23*, 3381−3399.
(7) Hagfedt, A.; Grätzel, M. *Acc. Chem. Res.* **2000**, *33*, 269−277.
(8) Benko, G.; Kallioinen, J.; Korppi-tommola, J. E. I.; Yartsev, A. P.; Sundstrom, V. *J. Am. Chem. Soc.* **2002**, *124*, 489−493.
(9) Asbury, J. B.; Anderson, N. A.; Hao, E.; Ai, X.; Lian, T. *J. Phys. Chem. B.* **2003**, *107*, 7376−7386.
(10) Kuciauskas, D.; Monat, J. E.; Villahermosa, R.; Gray, H. B.; Lewis, N. S.; McCusker, J. K. *J. Phys. Chem. B* **2002**, *106*, 9347−9358.
(11) Watson, D. F.; Meyer, G. J. *Annu. Rev. Phys. Chem.* **2005**, *56*, 119−156.
(12) Bram, O.; Cannizzo, A.; Chergui, M. *Phys. Chem. Chem. Phys.* **2012**, *14*, 7934−7937.
(13) Pellnor, M.; Myllyperkiö, P.; Korppi-Tommola, J.; Yartsev, A.; Sundström, V. *Chem. Phys. Lett.* **2008**, *462*, 205−208.

(14) Benko, G.; Kallioinen, J.; Myllyperkiö, P.; Trif, F.; Korppi-tommola, J. E. I.; Yartsev, A. P.; Sundström, V. *J. Phys. Chem. B* **2004**, *108*, 2862−2867.
(15) Koops, S. E.; O'Regan, B. C.; Barnes, P. R. F.; Durrant, J. R. *J. Am. Chem. Soc.* **2009**, *131*, 4808−18.
(16) Wenger, B.; Grätzel, M.; Moser, J.-E. *J. Am. Chem. Soc.* **2005**, *127*, 12150−1.
(17) Bauer, C.; Boschloo, G.; Mukhtar, E.; Hagfeldt, A. *J. Phys. Chem. B* **2002**, *106*, 12693−12704.
(18) Katoh, R.; Furube, A.; Kasuya, M.; Fuke, N.; Koide, N.; Han, L. *J. Mater. Chem.* **2007**, *17*, 3190.
(19) Katoh, R.; Kasuya, M.; Kodate, S.; Furube, A.; Fuke, N.; Koide, N. *J. Phys. Chem. B* **2009**, *113*, 20738−20744.
(20) Katoh, R.; Kasuya, M.; Furube, A.; Fuke, N.; Koide, N.; Han, L. *Sol. Energy Mater. Sol. Cells* **2009**, *93*, 698−703.
(21) Heimer, T. A.; Heilweil, E. J.; Bignozzi, C. A.; Meyer, G. J. *J. Phys. Chem. A.* **2000**, *104*, 4256−4262.
(22) Manzoni, C.; Polli, D.; Cerullo, G. *Rev. Sci. Instrum.* **2006**, *77*, 23103.
(23) Fantacci, S.; Lobello, M. G.; De Angelis, F. *Chimia* **2013**, *67*, 121−128.
(24) Perdew, J. P.; Burke, K.; Ernzerhof, M. *Phys. Rev. Lett.* **1997**, *77*, 3865.
(25) Te Velde, G.; Bickelhaupt, F. M.; Baerends, E. J.; Fonseca Guerra, C.; van Gisbergen, S. J. A.J.; Snijders, G.; Ziegler, T. *J. Comput. Chem.* **2001**, *22*, 931.
(26) Becke, A. D. *J. Chem. Phys.* **1993**, *98*, 5648.
(27) Frisch, G. W. T. M. J.; Schlegel, H. B.; Scuseria, G. E.; Robb, M. A.; Cheeseman, J. R.; Montgomery, J. A.; , Jr., Vreven, T.; Kudin, K. N.; Burant, J. C.; Millam, J. M.; Iyengar, S. S.; Tomasi, J.; Barone, V.; Mennucci, B.; Cossi, M.; Scalmani, G.; Rega, N.; Petersso, G. A.; , and J. A. P. *Gaussian 03*, Revision C.02; Gaussian: Wallingford, CT, 2004.
(28) Vittadini, A.; Selloni, A.; Rotzinger, F. P.; Grätzel, M. *Phys. Rev. Lett.* **1998**, *81*, 2954.
(29) Lundqvist, M. J.; Nilsing, M.; Persson, P.; Lunell, S. *Int. J. Quantum Chem.* **2006**, *106*, 3214.
(30) De Angelis, F.; Fantacci, S.; Mosconi, E.; Nazeeruddin, M. K.; Grätzel, M. *J. Phys. Chem. C.* **2010**, *115*, 8825−8831.
(31) De Angelis, F.; Fantacci, S.; Selloni, A.; Nazeeruddin, M. K.; Grätzel, M. *J. Phys. Chem. C.* **2011**, *114*, 6054−6061.
(32) Damrauer, N. H.; Cerullo, G.; Yej, A.; Boussie, T. R.; Shank, C. V; McCusker, K. *Science* **1997**, *275*, 54.
(33) Redmond, G.; Fitzmaurice, D. *J. Phys. Chem.* **1993**, *97*, 1426−1430.
(34) Rothenberger, G.; Fitzmaurice, D.; Grätzel, M. *J. Phys. Chem.* **1992**, *96*, 5983−5986.
(35) Cappel, U. B.; Karlsson, M. K.; Pschirer, N. G.; Eickemeyer, F.; Schoneboom, J.; Erk, P.; Boschloo, G.; Hagfeldt, A. *J. Phys. Chem. C.* **2009**, *113*, 14595−14597.
(36) Nunzi, F.; Mosconi, E.; Storchi, L.; Ronca, E.; Selloni, A.; Grätzel, M.; De Angelis, F. *Energy Environ. Sci.* **2013**, *6*, 1221−1229.